

DEFORMATION AND ENERGY ABSORPTION DIAGRAMS FOR CELLULAR SOLIDS

S. K. MAITI¹†, L. J. GIBSON² and M. F. ASHBY¹

¹Cambridge University, Engineering Department, Trumpington Street, Cambridge CB2 1PZ, England and

²Department of Civil Engineering, University of British Columbia, Vancouver B.C., Canada

(Received 23 May 1984)

Abstract—The mechanical properties of 3 types of cellular solids (flexible, plastic and brittle) have been measured as a function of density. The results are compared with models for the stiffness, strength and densification; and constitutive laws are developed. Data and models for each type of cellular solid are combined to develop *mechanism-mode maps* which summarise the properties in a single diagram; this understanding, in turn, allows the construction of *energy absorption diagrams* for classes of foams. Natural cellular materials fit the same pattern; maps are presented, as an example, for wood. The maps help in design and in the selection of the optimal foam for a given load-bearing or energy-absorbing application.

Résumé—Nous avons mesuré les propriétés mécaniques de trois types de solides cellulaires (flexible, plastique et fragile) en fonction de la densité. Nous comparons les résultats avec des modèles de la raideur, de la résistance et de la densification; nous présentons des lois constitutives. Nous combinons les résultats et les modèles pour chaque type de solide cellulaire afin de développer des cartes mécanisme-mode qui résument les propriétés en un diagramme unique; ceci permet à son tour de construire des diagrammes d'absorption d'énergie pour des classes d'écume. Les matériaux cellulaires naturels vérifient les mêmes diagrammes; nous présentons ainsi, par exemple, les diagrammes pour le bois. Ces cartes aident à concevoir et à choisir l'écume optimale pour une application donnée de support de charge ou d'absorption d'énergie.

Zusammenfassung—Die mechanischen Eigenschaften von drei Typen zellartiger Festkörper (flexibler, plastischer und spröder Typ) wurden in Abhängigkeit von der Dichte gemessen. Die Ergebnisse werden mit Modellen für die Steifheit, die Festigkeit und die Verdichtung verglichen; Grundgesetze werden entwickelt. Ergebnisse und Modelle werden für jeden zellartigen Festkörper so kombiniert, daß die Eigenschaften jeweils in einem einzigen Diagramm dargestellt werden kann. Daraus lassen sich wiederum Energieabsorptionsdiagramme für Klassen von Schäumen konstruieren. Natürliche zellartige Materialien fügen sich ein; z.B. wird ein Diagramm für Holz vorgelegt. Diese Diagrammkarten helfen bei dem Design und der Auswahl des optimalen Schaumes für eine gegebene Anwendung in Belastung oder Energieabsorption.

1. INTRODUCTION

Polymeric foams have certain characteristic mechanical properties. *Elastomeric or flexible foams*, in simple compression, are linear-elastic to a strain of about 5%. Then the cell walls buckle and the foam collapses at a nearly constant stress (giving a non-linear elastic deformation) until the cell walls touch and the stress-strain curve rises steeply. *Rigid polymers and metals*, when foamed, have a similar stress-strain curve, but for a different reason. Like flexible foams, they are linear-elastic to a strain of roughly 5%. Then they suffer plastic collapse, compressing plastically at a nearly constant stress until the cell walls touch, and the stress-strain curve rises steeply. *Brittle foams*, too, show an initial linear-elastic regime. But when the stress is reached at which cell walls fracture, the stress-strain curve becomes irregular (though roughly horizontal) and the foam crushes at (roughly) constant load.

Figure 1 shows, schematically, the structure of cellular solids. Some have *open cells*: the solid material is distributed as little beams which form the cell edges. Others have *closed cells*: the solid is distributed as little plates which form the cell faces. The mechanical properties reflect, to some extent, this distribution. In practice, most man-made foams (even those with closed cells faces) behave as if they had open cells because surface tension draws much of the solid material into the cell-edges during manufacture. For this reason, we discuss open-cell foams in detail, but treat closed cell foams only in passing.

The mechanical properties of a cellular solid can be related to the mechanics of bending, buckling, plastic collapse and brittle fracture of its cell walls. Each part of the stress-strain curve can be modelled [1-4]. The models give equations for Young's modulus E^* , the elastic buckling stress σ_a^* , the plastic collapse stress σ_p^* , the crushing strength σ_f^* , and terminal rise in strength, in terms of the density and properties of the material of which the foam is made.

†On leave from I.T.T., Bombay, India.

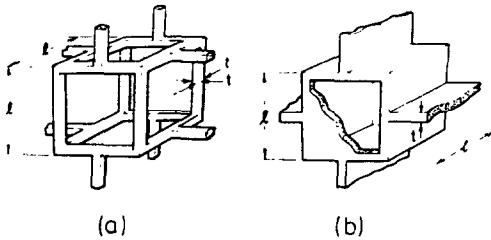


Fig. 1. Schematic of cellular material, showing dimensions.

This paper seeks to test and extend these models, (checking them against data from literature and new data, described below), to derive constitutive laws for design with cellular solids, and to develop diagrams which summarise the overall mechanical response of each type. Symbols are defined in Table 1.

2. EXPERIMENTAL RESULTS

2.1. Foamed plastics and ceramics

We tested samples of commercial flexible foams (a polyethylene and a polyurethane), samples of a commercial rigid foam (a polymethacrylimid) and an experimental batch of a brittle ceramic foam (mullite). The materials, their origins and the properties of the cell walls are listed in Table 2. Their structures are shown in Fig. 2.

Compression tests were carried out on blocks of foam of a convenient size (the size depending on the stiffness), at a temperature of 18°C and a strain-rate of roughly 2×10^{-3} /s. Results are shown in Figs 3–6. The axes are the nominal stress (the load P divided by the initial section A_0)

$$\sigma = \frac{P}{A_0} \quad (1)$$

and the nominal compressive strain

$$\varepsilon = \frac{h_0 - h}{h_0} \quad (2)$$

where h is the height of the sample after a strain ε , and h_0 is the original height. When foams are compressed beyond a strain of a few percent there is almost no lateral spreading, so the nominal and true stresses are, for all practical purposes, identical. The nominal compressive strain is, of course, limited to the range 0–1.

All the stress–strain curves show three regions: a *linear elastic region*; a long *plateau* where the stress is almost independent of strain; and (for all but the brittle foams) a final region of *densification* in which the stress–strain curve rises steeply. Young's modulus E^* of the rigid foams was measured by using clip gauges. The density ρ of each foam was measured by conventional methods. Mean values of ρ , E^* and of the plateau stress σ^* are listed in Table 3.

2.2. Woods

We also tested a number of woods, chosen to give a range of relative densities between 0.05 and 0.5. Samples of well-seasoned woods, roughly 20 mm \times 20 mm \times 40 mm, were cut with the long direction parallel to a radius of the trunk and parallel to the axis of the trunk. The samples were stored for 10 days to reach equilibrium moisture content (roughly 12%) and tested in compression at 18°C and a strain rate close to 10^{-3} /s. Results are shown in Figs 7 and 8.

Table 1. Symbols and units

σ	applied compressive stress (N/m ²)
ε	nominal compressive strain (–)
ε_0	strain at linear-elastic limit (–)
ε_c	strain at boundary between plateau and densification (–)
ρ	initial density of cellular solid (kg/m ³)
$\rho(\varepsilon)$	density after compressive strain ε (kg/m ³)
ρ_s	density of cell wall material (kg/m ³)
ρ/ρ_s	relative density (–)
E^*	Young's modulus of cellular solid (N/m ²)
E_s	Young's modulus of cell-wall material (N/m ²)
σ_{el}^*	elastic collapse or plateau stress of elastomeric foam (N/m ²)
σ_{pl}^*	plastic collapse or plateau stress of plastic foam (N/m ²)
σ_s	yield strength of cell-wall material (N/m ²)
σ_f^*	crushing stress of brittle foam (N/m ²)
σ_f	modulus of rupture of cell-wall material (N/m ²)
t	cell wall thickness (m)
l	cell size or cell wall length (m)
$l(\varepsilon)$	length of cell walls which are about to buckle at strain ε (m)
l_0	length of uncollapsed cell walls which buckle first (m)
I	second moment of area of cell wall or edge (m ⁴)
F	force acting on a cell wall (N)
F_{cr}	Euler buckling load for cell wall (N)
M_p	fully plastic moment of cell wall (Nm)
M_f	moment which will just fracture cell wall (Nm)
C_1 – C_3	dimensionless constants (–)
h_0	initial height of sample (m)
h	height after strain ε (m)
P	load (N)
W	energy absorbed per unit volume (J/m ³)

Table 2. Foam materials and the cell-wall properties

Material	Density range (kg/m ³)	ρ_s (kg/m ³)	E_s (MPa)	σ_s (MPa)	σ_f (MPa)	Source of materials
Flexible polyethylene	29–360	1200	700	—	—	"Frelen"
Flexible polyurethane	14–52	1100	45	—	—	"Dunlopillo", Dunlop Ltd, G.B.
Polymethylacrylamid	34–186	1200	3600	360	—	"Rohacell", Rohm GmbH, W. Germany
Brittle mullite	100–320	3200	3600	—	4	Morgan Thermic Ltd, G.B.
Woods						
(radial compression)	103–787	1500	10,000	135	—	} Commercial suppliers of seasoned woods
(axial compression)	103–764	1500	35,000	135	—	

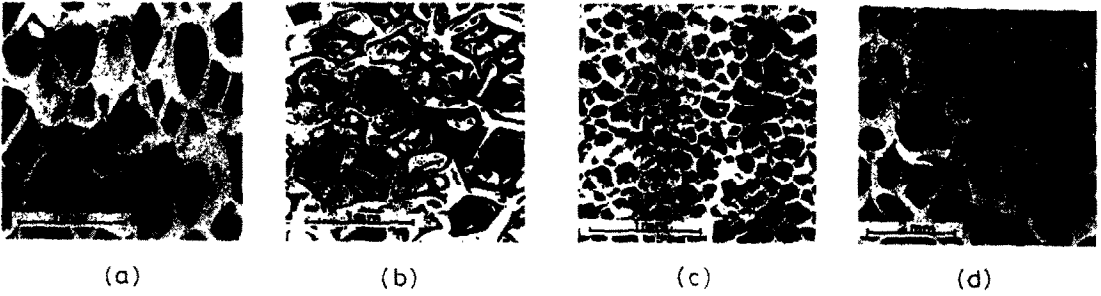


Fig. 2. Microstructures of the four types of foam: (a) polyethylene $\rho/\rho_s = 0.115$; (b) polyurethane $\rho/\rho_s = 0.029$; (c) polymethacrylimid $\rho/\rho_s = 0.103$; (d) mullite $\rho/\rho_s = 0.062$.

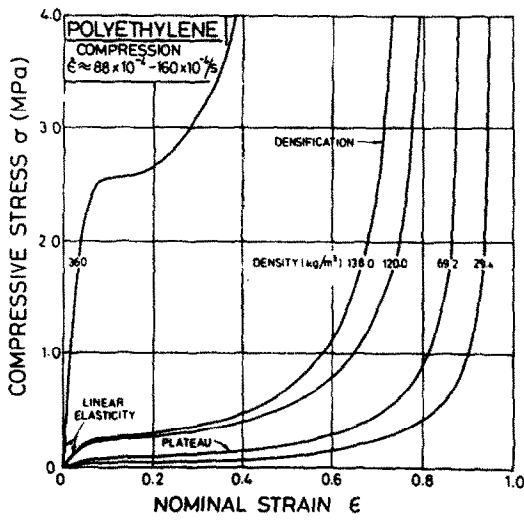


Fig. 3. Compressive stress-strain curves for flexible polyethylene foams.

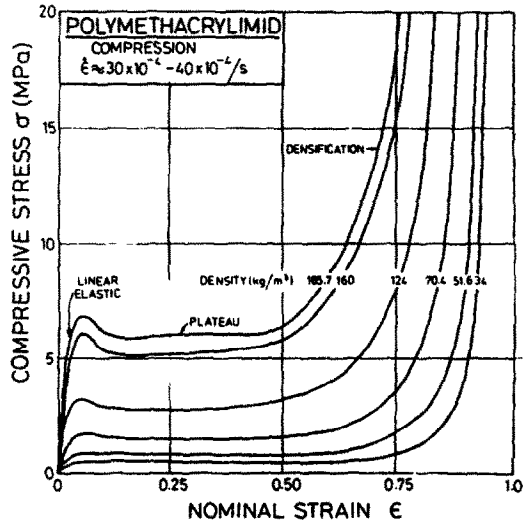


Fig. 5. Compressive stress-strain curves for rigid (plastic) polymethacrylimid foams.

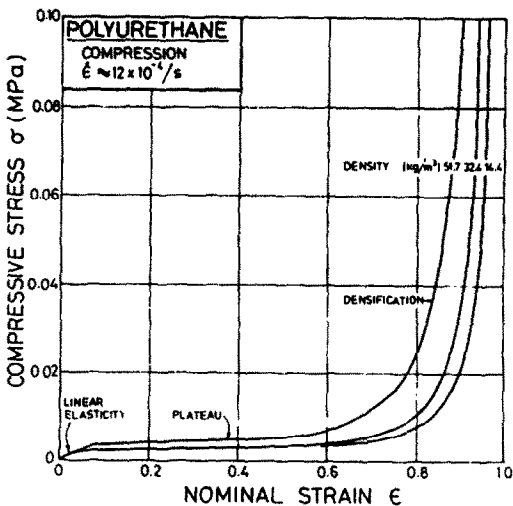


Fig. 4. Compressive stress-strain curves for flexible polyurethane foams.

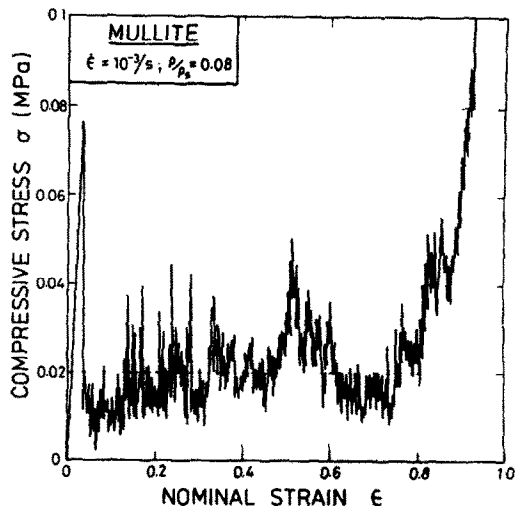


Fig. 6. Compressive stress-strain curve for a brittle mullite foam.

Table 3. Experimental measurements

Sample	ρ (kg/m ³)	E^* (MPa)		σ^* (MPa)		
<i>Elastomeric foams</i>						
Dunlop	D1	14.4	0.054	0.002		
	D14	32.4	0.062	0.0025		
	D17	51.7	0.057	0.005		
Frelen	F30	29.4	0.275	0.04		
	F70	69.2	1.10	0.1		
	F120	120.0	3.82	0.24		
	F175	138	4.58	0.3		
	F250	360	23.45	2.56		
	<i>Plastic foams</i>					
Rohacell	31	34	<i>Tension</i> 43	<i>Compr.</i> 20.8	0.4	
	51	51.6	73.4	28.1	0.8	
	71	70.4	95.2	56.9	1.6	
	110	124	194	129.7	3.0	
	170	160	280	198.7	5.2	
	190	185.7	432	258.9	6.0	
<i>Brittle foams</i>						
S1	100	8-50		0.02-0.18		
	200	6-22		0.035-0.16		
	280	2-8		0.072-0.21		
	320	25-44		0.093-0.16		
<i>Woods</i>						
Balsa	<i>Radial</i>	<i>Axial</i>	<i>Radial</i>	<i>Axial</i>	<i>Radial</i>	<i>Axial</i>
	103	103	31	420	0.80	8.0
Balsa	124	124	79	258	1.20	7.0
	403	355	198	1270	3.70	22.0
Pine	443	—	647	—	6.50	—
Willow	520	385	321	2203	8.25	22.5
	615	—	610	—	—	—
Beech	711	735	1160	7393	—	50.0
Beech	737	764	1569	7500	—	50.0

3. MODELS FOR THE MECHANICAL PROPERTIES

When a cellular material is compressed, the cell walls deform. The deformation modes (bending, buckling, plastic collapse and fracture) are known from studies of model cells [2]. Two-dimensional models (shown in insets of subsequent figures) can be analysed accurately [2]. With this knowledge, a kind of dimensional analysis of 3-dimensional cellular solids [1, 3, 4] becomes possible. This analysis, summarised briefly below, involves, in each case, a single geometric constant which must be determined by

experiment. The data are analysed to give this constant.

3.1. Stiffness

When a foam is loaded, the cell walls at first *bend* [1, 2, 5-7] as shown in the inset of Fig. 9. A force *F*, applied as shown, causes the non-vertical beams to deflect by an amount, δ , which can be calculated from elastic beam theory

$$\delta = \frac{C_1 F l^3}{E_s I} \tag{3}$$

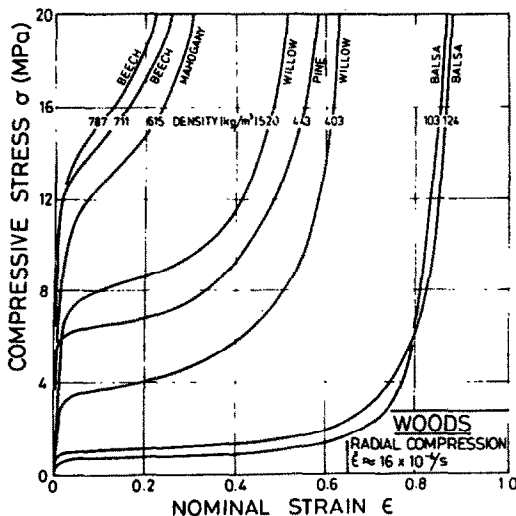


Fig. 7. Compressive stress-strain curves for woods in the radial direction (perpendicular to the grain).

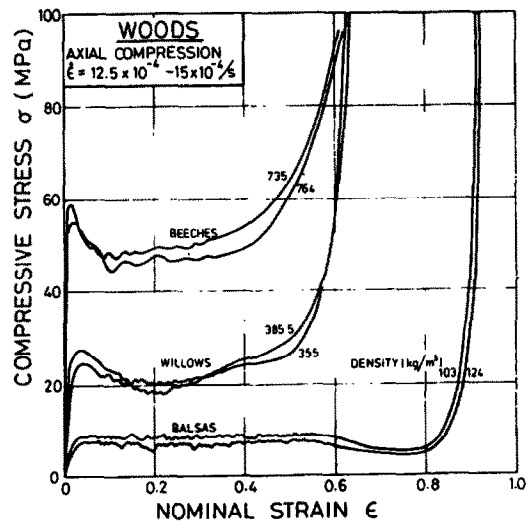


Fig. 8. Compressive stress-strain curves for woods in the axial direction (parallel to the grain).

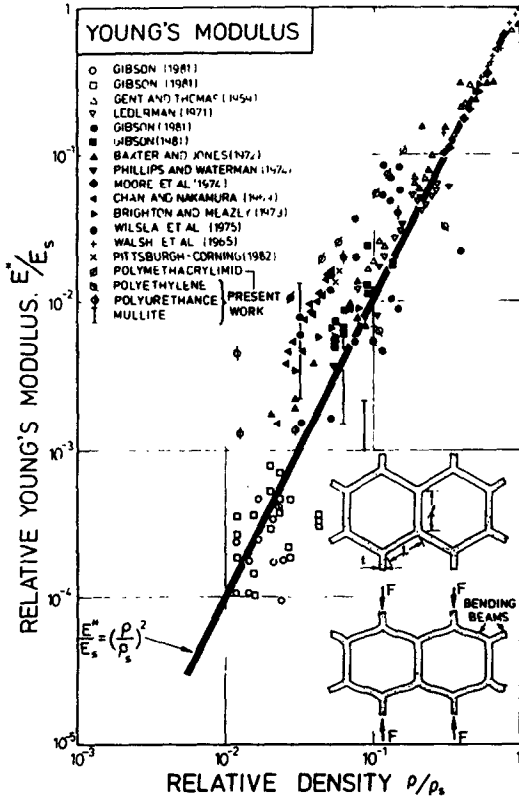


Fig. 9. The relative Young's modulus, E^*/E_s , plotted against relative density, ρ/ρ_s .

Here C_1 is a factor which depends on cell-wall geometry. A similar deflection occurs in a 3-dimensional cellular solid, like those shown in Fig. 1. Considering the open-cell foam, the force F is proportional to σl^2 where σ is the remote stress; and the strain ϵ is proportional to δ/l . The second moment of area, I , of a cell edge with section t^2 is t^4 so that the modulus E^* of the foam is

$$E^* \propto E_s \frac{t^4}{l^4}. \quad (4)$$

The dimensions of the open cells are related to the relative density of the foam ρ/ρ_s , by

$$\rho/\rho_s \propto t^2/l^2 \quad (5)$$

giving

$$\frac{E^*}{E_s} = C_2 \left(\frac{\rho}{\rho_s} \right)^2 \quad (6)$$

where C_2 is a constant. The shear modulus scales in a similar way, because shear deformation in a foam also causes simple bending of the cell walls. [For closed cells, $I \propto t^3$ and $\rho/\rho_s \propto t/l$ giving instead $E^*/E_s \propto (\rho/\rho_s)^3$.]

Data are compared with equation (6) in Fig. 9. The full line is a plot of equation (6) with $C_2 = 1$. It gives a good description of a wide range of materials and densities. (We find that plastic foams deviate systematically towards the line $E^*/E_s = (\rho/\rho_s)^{3/2}$, because,

we believe, some limited plasticity occurs even under small loads. Section 3.3, below, explains the power of $3/2$.)

Poissons ratios ν have been measured for cellular solids [1, 3]. In the linear-elastic regime, $\nu \approx 1/3$, although in the plateau regime it is almost zero.

3.2. Elastic buckling

Flexible foams show extensive non-linear elasticity. It is caused by the *elastic buckling* of the cell walls [8, 18], as shown in the inset of Fig. 10, and it is this that gives the plateau of the stress-strain curve for elastomeric foams.

The critical load at which a column of length l , Young's modulus E_s and second moment of area I buckles, is given by Euler's formula:

$$F_{cr} \propto \frac{E_s I}{l^2}. \quad (7)$$

If this load is reached for a layer of cells spanning the section, they buckle, initiating the *elastic collapse* of the foam. For the 3-dimensional open-cell foam of Fig. 1 the stress σ_{el}^* at which this occurs is proportional to F_{cr}/l^2 . Using the facts that $I \propto t^4$ and $\rho/\rho_s \propto (t/l)^2$ we obtain the elastic collapse, or plateau, stress

$$\frac{\sigma_{el}^*}{E_s} = C_3 \left(\frac{\rho}{\rho_s} \right)^2. \quad (8)$$

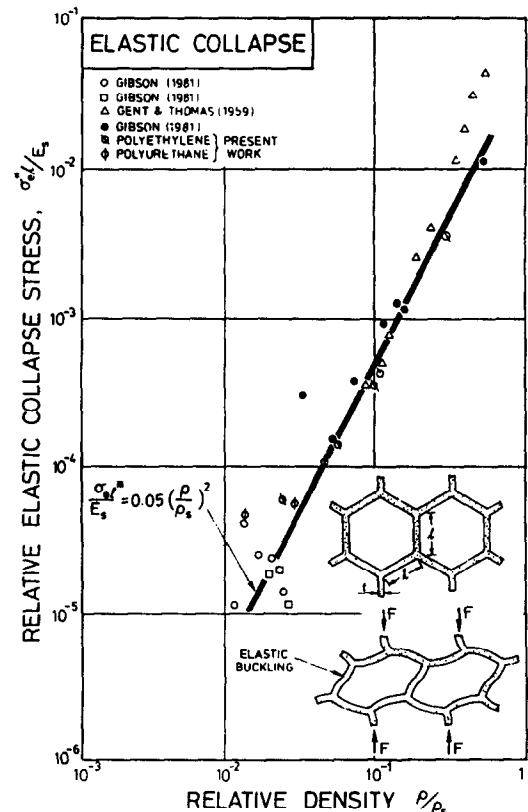


Fig. 10. The relative elastic collapse stress, σ_{el}^*/E_s , plotted against relative density, ρ/ρ_s .

It is valid for relative densities below 0.3. At higher densities, the cell walls are too short and stocky to buckle; instead they yield or crush.

Data for σ_{pl}^* for elastomeric foams are compared with equation (8) in Fig. 10. They are well fitted by the equation with $C_3 = 0.05$.

3.3. Plastic collapse

If the cell-wall material yields plastically, as do metals and many polymers, then the foam as a whole shows a plateau caused by plastic collapse. It occurs when the moment on the inclined cell walls exceeds the fully plastic moment, creating plastic hinges [2, 3, 19, 20] as shown in the inset of Fig. 11. For a beam of square section of side t , the fully plastic moment is

$$M_p = \frac{1}{4} \sigma_y t^3. \tag{9}$$

The moment is proportional to Fl , and (as before) the force F is proportional to σl^2 . Combining these results with equation (5) we find the plastic collapse, or plateau, stress σ_{pl}^* to be

$$\frac{\sigma_{pl}^*}{\sigma_y} = C_4 \left(\frac{\rho}{\rho_s} \right)^{3/2}. \tag{10}$$

Data for the plateau-stress of plastic foams are plotted in Fig. 11. They are well fitted by equation (10) with $C_4 = 0.3$ for relative densities less than 0.3 (1); at higher densities the cell edges are too short and stocky to bend plastically; instead, they shear.

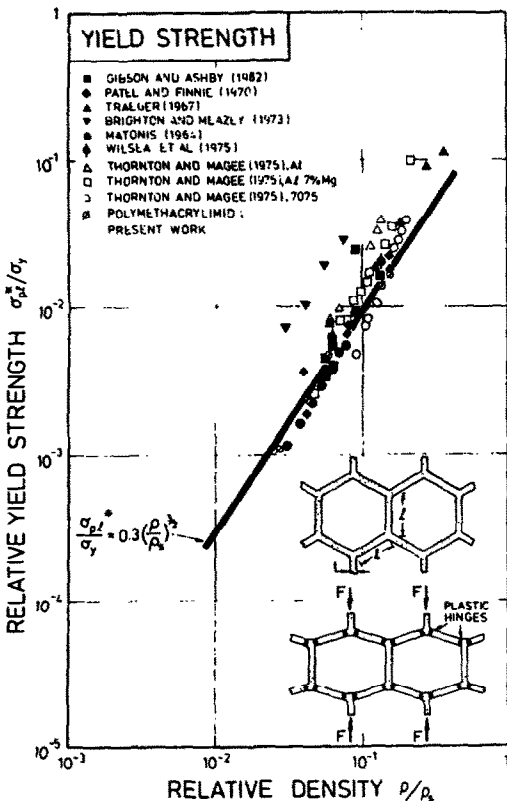


Fig. 11. The relative plastic collapse stress, σ_{pl}^*/σ_y , plotted against relative density, ρ/ρ_s .

3.4. Brittle crushing

Brittle foams (ceramics, and certain rigid polymers) collapse by yet other mechanisms: brittle crushing in compression [23], brittle fracture in tension [24, 25]. Let the modulus of rupture (the maximum surface or skin stress at the instant of fracture) for the cell-wall material be σ_f . Then a cell wall will fail as shown in the inset to Fig. 12 when the moment acting on it exceeds

$$M_f = \frac{1}{6} \sigma_f t^3.$$

The moment due to F is proportional to Fl , and the stress to F/l^2 . Combining these with equation (5) gives the crushing strength σ_f^* of the foam

$$\frac{\sigma_f^*}{\sigma_f} = C_7 \left(\frac{\rho}{\rho_s} \right)^{3/2}. \tag{11}$$

The limited experimental data, shown in Fig. 12, are consistent with $C_7 = 0.65$ but are insufficient to give much more confidence in equation (11). But observations, reviewed elsewhere [4], suggest that the model has the correct physical basis, and we shall employ it in subsequent sections.

3.5. Densification and the shape of the stress-strain curve

The plateau ends when the folding cell walls begin to touch. During elastic buckling or plastic collapse, the foam compresses axially with almost no lateral spreading ($\nu \approx 0$). Then simple geometry gives the

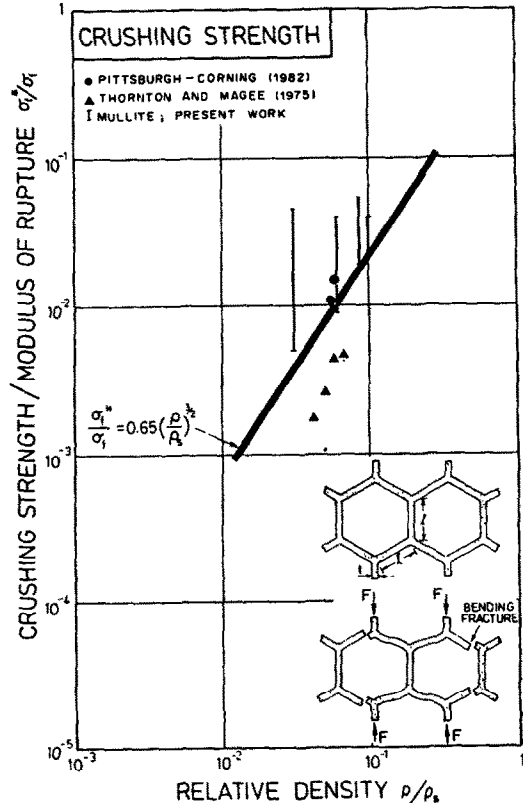


Fig. 12. The relative crushing strength, σ_f^*/σ_f , plotted against relative density, ρ/ρ_s , for brittle foams.

relative density $\rho(\varepsilon)/\rho_s$, after a nominal compressive strain ε as

$$\frac{\rho(\varepsilon)}{\rho_s} = \frac{\rho}{\rho_s} \left(\frac{1}{1-\varepsilon} \right) \quad (12)$$

where ρ/ρ_s is the initial relative density. Densification is complete, and the stress-strain curve becomes almost vertical, when $\rho(\varepsilon)/\rho_s = 1$, when the strain is

$$\varepsilon_f = 1 - \rho/\rho_s. \quad (13)$$

We find experimentally that the end of the plateau corresponds to $\rho(\varepsilon)/\rho_s \approx 0.33$ (the solid occupies $\frac{1}{3}$ of the total volume) when the strain is

$$\varepsilon_s = 1 - 3(\rho/\rho_s). \quad (14)$$

Consider now the shape of the stress-strain curve for flexible foams. In any sample of the foam, there is a distribution of cell edge-lengths and angles. The plateau starts when a layer of cells (those with longest, or most favourably oriented, edges) buckle [equation (7)]. A small increase in stress is needed to cause more cell edges (those which are slightly shorter) to buckle. We postulate that the length of the edges which are about to buckle after a strain ε , $l(\varepsilon)$, is given by

$$l(\varepsilon) = l_0 \frac{\left[1 - \left(\frac{\rho(\varepsilon)}{\rho_s} \right)^{1/3} \right]}{1 - (\rho/\rho_s)^{1/3}} \quad (15)$$

[The value $l(\varepsilon)$ ranges from l_0 at the start of deformation to zero when full density is reached.] Using equation (12) we obtain

$$l(\varepsilon) = l_0 \frac{\left[1 - \left(\frac{\rho}{\rho_s} \frac{1}{1-\varepsilon} \right)^{1/3} \right]}{1 - (\rho/\rho_s)^{1/3}}. \quad (16)$$

The argument of Section 3.2 can now be repeated. The force F on the cell wall is related to l_0 throughout the test by $F = \sigma l_0^2$. Collapse of cells with edge length $l(\varepsilon)$ [given by equation (16)] occurs when this force exceeds the buckling load given by equation (7). Combining these equations gives

$$\frac{\sigma}{E_s} = 0.05 \left(\frac{\rho}{\rho_s} \right)^2 \left\{ \frac{1 - (\rho/\rho_s)^{1/3}}{1 - \left[\frac{\rho/\rho_s}{1-\varepsilon} \right]^{1/3}} \right\}^2 \quad (17)$$

which reduces to our original equation (8) at small strains, but becomes infinite (approximating E_s) at the strain given by equation (13).

A similar analysis can be made for plastic foams. We postulate that the length of the beams which are about to bend plastically decreases as strain proceeds (because the long ones bend first). If the length at a strain ε is given (as before) by equation (16), then by

the argument of Section 3.3, the strength of a plastic foam follows

$$\frac{\sigma}{E_s} = 0.3 \frac{\sigma_y}{E_s} \left(\frac{\rho}{\rho_s} \right)^{3/2} \left\{ \frac{1 - (\rho/\rho_s)^{1/3}}{1 - \left[\frac{\rho/\rho_s}{1-\varepsilon} \right]^{1/3}} \right\}. \quad (18)$$

This reduces to equation (10) at small strains, but becomes infinite (approximating E_s) as the foam is compressed to the solid density [equation (13)].

These two results give an approximate description of the stress-strain curves for flexible and for rigid-plastic foams, in the fields of plastic collapse and densification. They are combined with the equations for linear-elasticity, in the next sections, to construct deformation-mode maps and energy-absorption diagrams.

4. CONSTRUCTION OF DEFORMATION-MODE MAPS

We have seen that when an elastomeric foam is compressed, it first deforms in a linear-elastic way; then its cells buckle to give non-linear elasticity; and, finally, the cells collapse completely and the stress rises rapidly as their faces and edges are forced together. A plastic foam behaves in a somewhat similar way, except that linear elasticity is now followed by plastic collapse, and the ultimate forcing together of the cell walls. With brittle foams, progressive crushing can again lead to a plateau which ends when the material is completely crushed. We have seen, too, that each of these processes can be modelled adequately by using classical beam theory to analyse the deformation of cell walls. The analysis relates foam properties to the relative density (ρ/ρ_s) and to the properties of the material of which the foam is made. The relations, summarised in Table 4, suggest a normalisation which brings the properties of foams with the same relative densities into coincidence. Then the properties of an entire family of foams can be shown as a *deformation mode map* (4), of which Figs 13–16 are examples. The map has axes of normalised compressive stress σ/E_s , and the compressive strain ε . It shows the *fields* in which each mode of deformation (linear elasticity, non-linear elasticity, plastic collapse and so forth) is dominant. Superimposed on the fields are *stress-strain contours for constant (initial) relative density*.

4.1. Elastomeric foams

Figures 13 and 14 show mechanism-mode maps for elastomeric foams. Figure 13 shows the experimental stress-strain curves for polymeric foams; Fig. 14 is based on the theory alone. Mechanism field boundaries (heavy lines) are shown on both figures. They were constructed as follows.

The linear-elastic regime ends when elastic buckling begins. Using equations (6) and (8), and the fact that $\sigma = E\varepsilon$ in the linear-elastic region, we obtain the

Table 4. Equation for stiffness and strength of cellular solids

Property	Equation	Equation No.
Young's modulus	$\frac{E^*}{E_s} = \left(\frac{\rho}{\rho_s}\right)^2$	(6)
Plateau stress, flexible foams	$\frac{\sigma_{\epsilon_1}^*}{E_s} = 0.05 \left(\frac{\rho}{\rho_s}\right)^2$	(8)
Plateau stress, plastic foams	$\frac{\sigma_{pl}^*}{\sigma_y} = 0.3 \left(\frac{\rho}{\rho_s}\right)^{3/2}$	(10)
Approximate plateau stress, brittle foams	$\frac{\sigma_f^*}{\sigma_f} = 0.65 \left(\frac{\rho}{\rho_s}\right)^{3/2}$	(11)
Stress-strain response, flexible foam	$\frac{\sigma}{E_s} = 0.05 \left(\frac{\rho}{\rho_s}\right)^2 \left\{ \frac{1 - \left(\frac{\rho}{\rho_s}\right)^{1/3}}{1 - \left[\frac{\rho}{\rho_s} \left(\frac{1}{1-\epsilon}\right)\right]^{1/3}} \right\}^2$	(17)
Stress-strain response, plastic foam	$\frac{\sigma}{\sigma_y} = 0.3 \left(\frac{\rho}{\rho_s}\right)^{3/2} \left\{ \frac{1 - \left(\frac{\rho}{\rho_s}\right)^{1/3}}{1 - \left[\frac{\rho}{\rho_s} \left(\frac{1}{1-\epsilon}\right)\right]^{1/3}} \right\}$	(18)

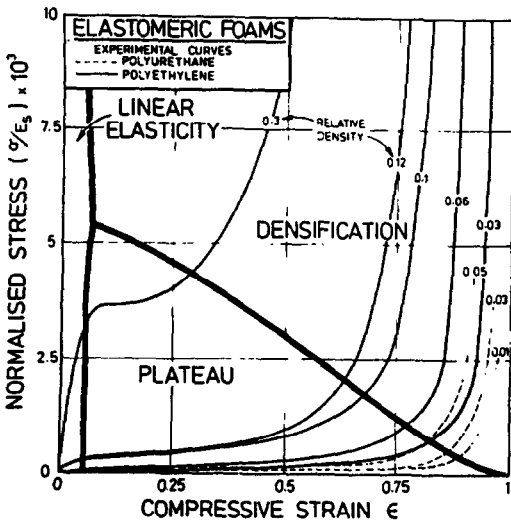


Fig. 13. A deformation-mode map for flexible foams. It shows the data of Figs 3 and 4, normalised. The construction of the field boundaries is described in the text.

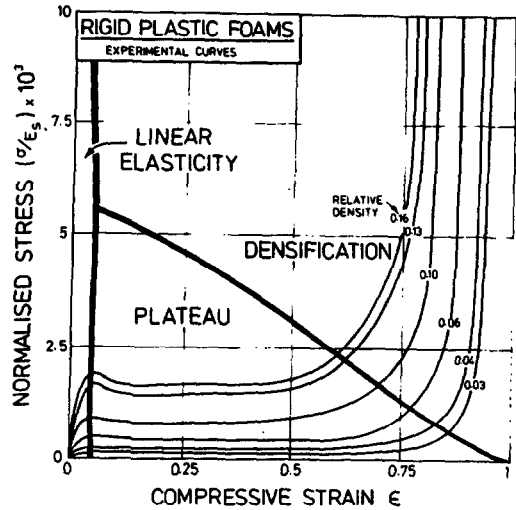


Fig. 15. A deformation-mode map for plastic foams. It shows the data of Fig. 5, normalised. The construction of the field boundaries is described in the text.

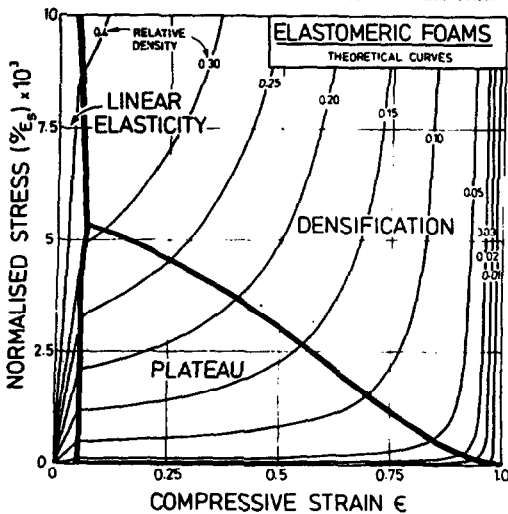


Fig. 14. A deformation-mode map for flexible foams, constructed entirely from the equations developed in the text.

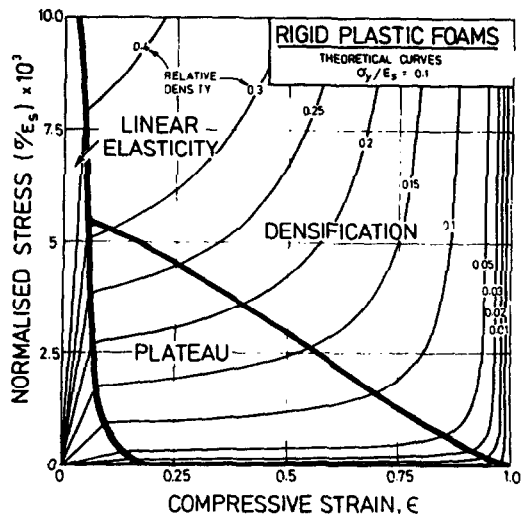


Fig. 16. A deformation-mode map for plastic foams, constructed entirely from the equations developed in the text.

strain corresponding to the boundary of the linear-elastic field

$$\varepsilon = C_3 = 0.05$$

At relative densities above about 0.3 the cell walls become so stocky that they can no longer buckle elastically. The field boundary thus bends until it is tangent to the linear-elastic loading line for $\rho/\rho_s = 0.3$.

Once elastic buckling starts, the stress is related to the strain by equation (17). We define the transition from buckling to densification as the line at which the relative density has reached $\frac{1}{3}$. Then, from equations (14) and (17) the equation of the transition is

$$\frac{\sigma}{E_s} = 5.9 \times 10^{-2} (1 - \varepsilon)^2 \left\{ 1 - \left(\frac{1 - \varepsilon}{3} \right)^{1/3} \right\}^2. \quad (19)$$

It is plotted as a heavy line, sloping down from left to right on the figures.

Figure 14 shows a theoretical map. The contours are stress-strain curves for foams of relative density between 0.01 and 0.4. They show a linear elastic regime [equation (6)] and a plateau corresponding to elastic buckling; they start to bend upwards when densification starts [equation (17)]; and they approach a limiting slope of E_s when densification is complete [equation (13)]. Within the field of elastic buckling the material exists in two states at almost the same stress (the linear-elastic state and the densified state); it is like the p - V response of an ideal gas (or the temperature-entropy diagram for steam) in which gas and liquid states can co-exist. The material deforms by the formation of densified bands which thicken, at constant stress, as the strain is increased, until the entire material has reached the dense state.

The figure describes the overall response of all isotropic, flexible foams in compression. In tension, flexible foams are roughly linear-elastic to rupture.

4.2. Rigid plastic foams

Plastic foams, like the elastic ones, show three regions: linear elasticity, plastic collapse and densification—though now the strain beyond the linear-elastic regime is not recoverable. Figures 15 and 16 are a pair of maps, one showing our experimental stress-strain curves for plastic foams, the other, based on the theory alone. Mechanism field-boundaries are superimposed on the stress-strain curves.

The boundary of the linear-elastic field (heavy line) is obtained from the equation for linear elasticity [equation (6)] and that for plastic collapse [equation (10)]; its equation is

$$\frac{\sigma}{E_s} = \left(0.3 \frac{\sigma_y}{E_s} \right)^4 \frac{1}{\varepsilon^3}. \quad (20)$$

In constructing the map we have taken σ_y/E_s to be 0.10 (a fairly typical value). Next to the linear-elastic field is the field of plastic collapse. As before, two states of strain co-exist at almost the same stress, so

that complete collapse of part of the structure can occur while the rest is still elastic; the bands of dense material broaden with increasing strain. We define the transition from collapse to densification as the line at which the relative density has reached $\frac{1}{3}$. Then, from equation (14) and equation (18), the equation of the transition line is

$$\frac{\sigma}{E_s} = 0.19 \frac{\sigma_y}{E_s} (1 - \varepsilon)^{3/2} \left\{ 1 - \left(\frac{1 - \varepsilon}{3} \right)^{1/3} \right\}. \quad (21)$$

It is plotted as a heavy line sloping down from left to right on Figs 15 and 16.

Figure 16 shows a theoretical map for plastic foams with $\sigma_y/E_s = 0.10$. It shows fields of elastic deformation, plastic collapse and densification. Superimposed on the fields are stress-strain curves for foams with densities from 0.01 to 0.4.

The figure shows the overall response of isotropic, plastic foams in compression. It is less general than the map for elastomeric foams because it must be constructed for a particular value of σ_y/E_s . But the equations show that the boundaries are not very sensitive to its value, and, for a given material, the diagram shows the behaviour for all densities.

The behaviour of plastic foams in tension resembles that in compression, truncated by fracture.

4.3. Brittle foams

Rigid foams show linear-elastic behaviour to fracture. In compression, the foam crushes at constant stress [equation (11)], and since the crushing equation has the same form as that for plastic collapse, the behaviour will resemble that of Figs 15 and 16. If the foam is contained, it will densify at the strain given approximately by equation (18), with σ_y/E_s replaced by σ_f/E_s .

In tension, linear elastic behaviour is truncated by fast, brittle fracture. The fracture mechanics of foams [28] need not concern us here.

4.4. Woods

These ideas can be applied, in an approximate way, to the compressive deformation of wood. Woods are cellular solids, composed of mixed polymers (cellulose, lignin, hemicellulose), and with a relative density ranging from less than 0.05 (balsas) to almost 1 (lignum vitae). Compressed across the grain, wood behaves like a rigid-plastic foam. Stress-strain curves for the woods we tested are shown in Fig. 17, plotted on axes of σ/E_s and ε (data in Tables 2 and 3).

The field boundaries of Fig. 17 were constructed as follows. In radial compression, Young's modulus for woods is found to follow the same law as elastic foams (29)

$$E^* = 10 \left(\frac{\rho}{\rho_s} \right)^2 GN/m^2. \quad (22)$$

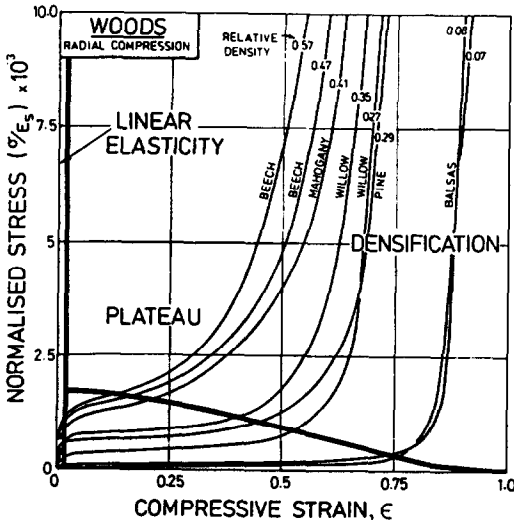


Fig. 17. A deformation-mode map for woods, tested in the radial direction (across the grain).

Compressive collapse in the radial direction equation (29) starts at the stress

$$\sigma^* = 135 \left(\frac{\rho}{\rho_s}\right)^2 \text{ MN/m}^2. \quad (23)$$

Thus the equation of the boundary separating elastic from collapse behaviour is

$$\epsilon = 0.014. \quad (24)$$

Using the method given in Section 3.5, the stress-strain beyond yield is described approximately by

$$\frac{\sigma}{E_s} = 0.014 \left(\frac{\rho}{\rho_s}\right)^2 \left\{ \frac{1 - \left(\frac{\rho}{\rho_s}\right)^{1/3}}{1 - \left[\frac{\rho}{\rho_s} \left(\frac{1}{1-\epsilon}\right)\right]^{1/3}} \right\}$$

and the boundary between collapse and densification, where the relative density reaches $\frac{1}{3}$, is given by

$$\frac{\sigma}{E_s} = 0.005 (1 - \epsilon)^2 \left[1 - \left(\frac{1 - \epsilon}{3}\right)^{1/3} \right]. \quad (25)$$

The field boundaries divide the behaviour into 3 regimes and give a diagram which summarises the properties of all woods in radial compression.

Compression along the grain is more complicated. In this direction, the wood has properties intermediate between those of a rigid-plastic and a brittle cellular solid (compare the stress-strain curves of Fig. 8 with those of Figs 5 and 6). In axial compression, Young's modulus varies linearly with density [29, 30]

$$E \approx 35 \left(\frac{\rho}{\rho_s}\right) \text{ GN/m}^2 \quad (26)$$

and the collapse stress σ^* , too, varies linearly with density [29, 30]

$$\sigma^* = 150 \left(\frac{\rho}{\rho_s}\right) \text{ MN/m}^2. \quad (27)$$

Then the equation of the line separating elastic and collapse behaviour is

$$\epsilon = 0.004.$$

When woods are compressed axially, they collapse by a process which involves the kinking [30] or fracture [29, 30] of the cell walls. This occurs at essentially constant stress until a critical state is reached, when the stress-strain curve bends sharply upwards. Experimentally, we find that the bend upwards occurs at a strain ϵ_c corresponding to a density of roughly 0.5

$$\epsilon_c = 1 - 2 \left(\frac{\rho}{\rho_s}\right). \quad (28)$$

Combining this with equation (27) gives the field boundary

$$\frac{\sigma^*}{E_s} = 2 \times 10^{-3} (1 - \epsilon). \quad (29)$$

It is plotted as a heavy line on Fig. 18. The figure summarises the compressive behaviour of woods in the axial direction. Both diagrams allow, by interpolation, or the use of the equations, the approximate prediction of the stress-strain curve for woods of other densities.

5. CONSTRUCTION OF ENERGY-ABSORPTION DIAGRAMS

The commonest use of foams is in packaging. The aim is to absorb energy (usually the kinetic energy) of the packaged object when it is dropped, or is accelerated or decelerated in some other way, while at the same time keeping the force on the object below the limit which will cause damage. In selecting a material for the package, we need to know the energy that can be absorbed without the stress exceeding a critical value. We show below that there is an optimum foam density for a given package. If

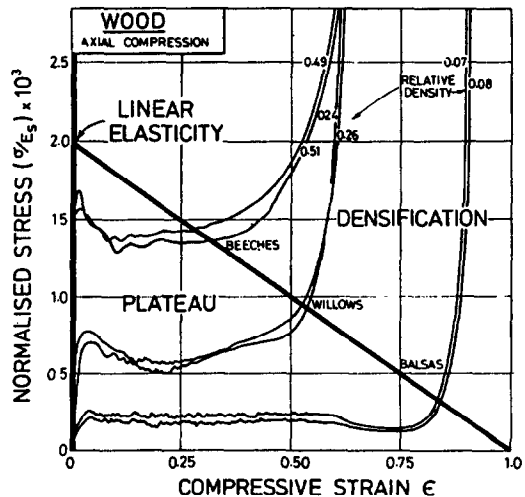


Fig. 18. A deformation-mode map for woods tested in the axial direction (along the grain).

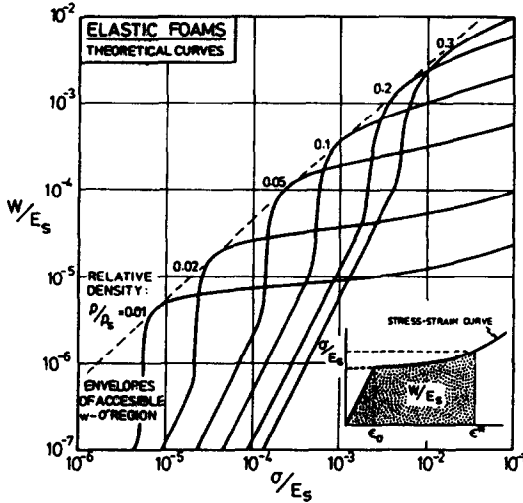


Fig. 19. An energy-absorption diagram for elastomeric foams, constructed from the equations given in the text. The broken line divides the diagram into an accessible and an inaccessible region.

the density is too low, the foam “bottoms out” (with a sharp increase in stress) before enough energy has been absorbed. If it is too dense, the stress exceeds the critical value before enough energy has been absorbed.

Figure 19 shows, inset, part of a stress-strain curve for a foam. It is linear-elastic to ϵ_0 , and thereafter follows the stress-strain $\sigma(\epsilon)$ curve described approximately by equation (17) or (18). The area, up to the strain ϵ^* , where the stress is σ , (shaded on Fig. 19) is

$$W = \int_0^{\epsilon_0} \sigma \, d\epsilon + \int_{\epsilon_0}^{\epsilon^*} \sigma(\epsilon) \, d\epsilon$$

or

$$\frac{W}{E_s} = \frac{1}{2} \frac{E^*}{E_s} \epsilon_0^2 + \int_{\epsilon_0}^{\epsilon^*} \frac{\sigma(\epsilon)}{E_s} \, d\epsilon \quad (30)$$

This equation was integrated using equation (17) for $\sigma(\epsilon)$ for elastic foams and equation (18) for plastic foams, to give Figs 19 and 21. Similar diagrams can, of course, be constructed directly from the experimental stress-strain curves (such as those shown in Figs 3-6) by measuring the area W/E_s , up to the strain ϵ^* corresponding to the stress σ/E_s . Such diagrams are shown, for comparison, in Figs 20 and 22.

The energy diagram, calculated for elastic foams (Fig. 19) shows the normalised energy absorbed per unit volume for foam, W/E_s , plotted against the peak stress σ/E_s , for a range of densities ρ/ρ_s . Normalised in this way, the diagram describes all elastic foams. If the critical damage stress is selected, then the diagram gives the foam density which will absorb the greatest amount of energy without this stress being exceeded. The lower the peak stress, the lower is the optimum foam density. As an example, using Fig. 19 or 20, the optimum foam density for a critical damage

stress $\sigma/E_s = 10^{-3}$ is $\rho/\rho_s = 0.1$. Choosing the right density is important: it can easily give a factor of 10 greater absorption of energy than a wrongly-chosen foam.

Figures 21 and 22 show energy diagrams for a plastic foam with $\sigma_y/E_s = 0.1$. Such diagrams are less general than those for elastic foams, because σ_y/E_s must be specified; but a single diagram still describes all foams made of a given material (polystyrene, for example). Here, too, there is an optimum foam density for a given energy absorption and peak stress. The diagram allows it to be chosen.

The figures show that, for a given material (and thus E_s), there is a maximum energy which can be absorbed for a given peak stress. The envelope shown as a broken line on Figs 19 and 21 divides the diagram into an accessible region (below the line) and an inaccessible one (above). For elastomeric foams, the equation of the line is approximately

$$W/E_s = 0.11 \left(\frac{\sigma}{E_s} \right)^{7/8} \quad (31)$$

It applies to all elastic foams. For the plastic foam with $\sigma_y/E_s = 0.1$, the equation of the line is approximately

$$W/E_s = 0.05 \left(\frac{\sigma}{E_s} \right)^{2/3} \quad (32)$$

The equations apply from $\rho/\rho_s = 0.01$ to $\rho/\rho_s = 0.3$.

6. CONCLUSIONS AND APPLICATIONS

6.1. Conclusions

When a cellular solid with a relative density below 0.30 is compressed, it shows a stress-strain curve with three parts: a linear-elastic part, a long plateau, and a regime of final densification. The properties of an entire class of such solids can be summarised as a

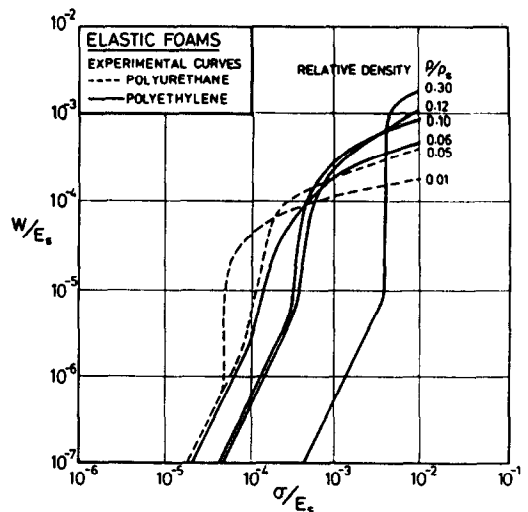


Fig. 20. An energy-absorption diagram for elastomeric foams, constructed by measuring the areas under the stress-strain curves of Figs 3 and 4. It is directly comparable with Fig. 19.

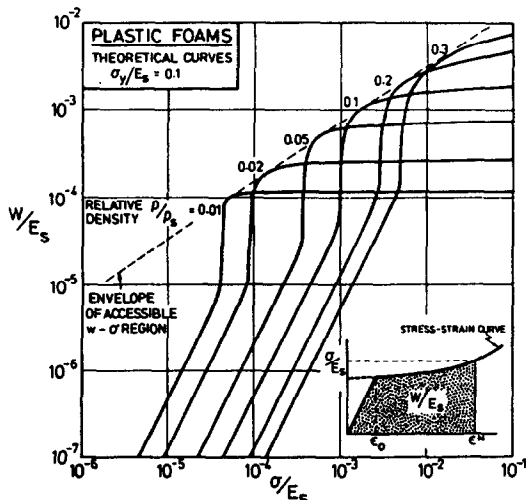


Fig. 21. An energy-absorption diagram for plastic foams, constructed from the equations given in the text, with $\sigma_y/E_s = 0.1$. The broken line divides the diagram into an accessible and an inaccessible region.

deformation-mode map, which shows how each of the three parts changes as the relative density changes. The method can be applied to man-made foams (Figs 13–16) and to natural materials, such as woods (Figs 17 and 18), to give diagrams which summarise the stress-strain response of each class of material.

The mechanical properties of cellular solids can be modelled with precision. The models lead to constitutive laws (stress-strain relations) which have been thoroughly tested in simple compression. They are summarised in Table 4. The constitutive laws can be used to construct deformation-mode maps, and can be integrated to construct energy-absorption diagrams. These diagrams (Figs 19–22) show how the energy absorbed, per unit volume of foam, depends on the density of the foam and on the stress. The

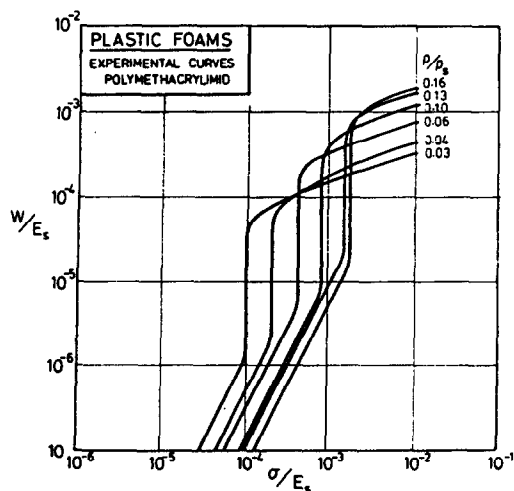


Fig. 22. An energy-absorption diagram for polymethacrylimid foams, constructed by measuring the areas under the stress-strain curves of Fig. 5. It is directly comparable with Fig. 21.

diagrams show that there is an optimum foam density for a given packaging or energy-absorbing application.

6.2. Design with cellular solids

The equations derived in the text, and summarised in Table 4, provide the basic information for design with foams in load-bearing applications. The tests described above all involved simple compression. Under multiaxial loads, the behaviour is more complicated. At small strains ($\epsilon < 5\%$), while the material is linear-elastic, it behaves like any other elastic solid [1, 3] with Young's modulus E^* given by equation (6) and Poisson's ratio $\nu = \frac{1}{3}$. But once the plateau-stress has been reached, the behaviour changes: the extensive deformation at nearly constant stress involves a large volume change, but almost no lateral strain [1, 3, 26, 27] so that $\nu \approx 0$. The material fails under a multiaxial state of stress when the maximum principal stress (not the octahedral shear stress) reaches the critical value of σ^* [equation (8) for flexible foams, equation (10) for plastic foams]. Because of this, the indentation hardness of plastic foams is equal to σ_{pl}^* (not $3\sigma_{pl}^*$ as in dense solids) and the force needed to compress a foam is the same whether it is free at its edges or constrained there [15]. Once densification starts, of course, the properties revert towards those of conventional solids.

The deformation mode map for a class of foams provides a compact summary of the mechanical response of the class. In particular, the maps give a rational way of selecting the material and density which will give a desired stress-strain response. Similarly, the energy-absorption diagram for a class of foam summarises the energy absorbing capacity of all members of the class. The diagrams identify the optimum foam material and density for a given packaging, padding or cushioning application.

Acknowledgements—We wish to thank Professor K. E. Easterling and Dr C. R. Calladine for many helpful discussions. We particularly wish to thank Mr John Godlonton for technical assistance and Trish Shepherd for typing the manuscript.

REFERENCES

1. L. J. Gibson, Ph.D. Thesis, Engineering Department, Cambridge University (1981).
2. L. J. Gibson, M. F. Ashby, G. S. Schajer and C. I. Robertson, *Proc. R. Soc. Lond.* **A382**, 25 (1982).
3. L. J. Gibson and M. F. Ashby, *Proc. R. Soc. Lond.* **A382**, 43 (1982).
4. M. F. Ashby, *Metall. Trans.* **14A**, 1755 (1983).
5. M. R. Patel and I. Finnie, *J. Mater.* **5**, 909 (1970).
6. W. L. Ko, *J. Cell. Plastics* **1**, 45 (1965).
7. G. Menges and F. Knipschild, *Polymer Engng Sci.* **15**, 623 (1975).
8. A. N. Gent and A. G. Thomas, *J. appl. Polymer Sci.* **1**, 107 (1959).
9. J. M. Lederman, *J. appl. Polymer Sci.* **15**, 693 (1971).
10. S. Baxter and T. T. Jones, *Plastics Polymers* **40**, 69 (1972).

11. P. J. Phillips and N. R. Waterman, *Polymer Engng Sci.* **4**, 67 (1974).
12. D. R. Moore, *The Use of Glass in Engineering*, Design Council Guide 05, Oxford Univ. Press (1980).
13. R. Chan and M. Nakamura, *J. Cell Plastics* **5**, 112 (1969).
14. C. A. Brighton and A. E. Mezey, *Expanded polyvinyl chloride*, in *Expanded Plastics—Trends in Performance Requirements*, Micro Symposium, Q.M.C. Industrial Research Ltd, London (1973).
15. M. Wilsea, K. L. Johnson and M. F. Ashby, *Int. J. Mech. Sci.* **17**, 457 (1975).
16. J. B. Walsh, W. F. Brace and A. W. England, *J. Am. Ceram. Soc.* **48**, 605 (1965).
17. *Foamglass Data Sheets*, Pittsburgh-Corning Inc. (1982).
18. A. M. Gent and A. G. Thomas, *Rubber Chem. Technol.* **36**, 597 (1963).
19. P. H. Thornton and C. L. Magee, *Metall. Trans.* **6A**, 1253 (1975).
20. P. H. Thornton and C. L. Magee, *Metall. Trans.* **6A**, 1801 (1975).
21. R. K. Traeger, *J. Cell. Plast.* **3**, 405 (1967).
22. V. A. Matonis, *Soc. Plast. Engng J.*, p. 1024 (1964).
23. K. C. Rusch, *J. appl. Polym. Sci.* **14**, 1263 (1970).
24. A. McIntyre and G. E. Anderton, *Polymer* **20**, 247 (1979).
25. C. W. Fowlkes, *Int. J. Fract.* **10**, 99 (1974).
26. M. C. Shaw and T. Sata, *Int. J. Mech. Sci.* **8**, 469 (1966).
27. J. A. Rinde, *J. appl. Polym. Sci.* **14**, 1913 (1970).
28. S. K. Maiti, M. F. Ashby and L. J. Gibson, *Scripta metall.* **18**, (3) (1984).
29. K. E. Easterling, R. Harrysson, L. J. Gibson and M. F. Ashby, *Proc. R. Soc. Lond.* **A383**, 31 (1982).
30. J. M. Dinwoodie, *Timber: Its Nature and Behaviour*. Van Nostrand, New York (1981).